



ELSEVIER

Earth and Planetary Science Letters 183 (2000) 457–469

EPSL

www.elsevier.com/locate/epsl

Some remarks on U–Th mineral ages from igneous rocks with prolonged crystallisation histories

Bruce Charlier^a, Georg Zellmer^{b,*}

^a Department of Earth Sciences, The Open University, Walton Hall, Milton Keynes MK7 6AA, UK

^b Department of Earth Sciences, University of Bristol, Wills Memorial Building, Queens Rd., Bristol BS8 1RJ, UK

Received 6 June 2000; received in revised form 2 October 2000; accepted 8 October 2000

Abstract

Mineral isochron dating is a frequently used geochronological tool. One of its assumptions is that the minerals grow over a time period that is small compared to the half-life of the radiogenic isotope system used. In recent years, increasing analytical precision has promoted the use of the short-lived U-series isotope system in order to date young crystallisation events. Three whole-rock zircon U–Th isochrons from the 26.5 ka Oruanui eruption in the Taupo Volcanic Zone, New Zealand, yield pre-eruptive model ages of 5.5 ± 0.8 ka, 9.7 ± 1.7 ka and 12.3 ± 0.8 ka for the sub-63 μm , 63–125 μm and 125–250 μm zircon size fractions, respectively. This suggests that in this case the assumption of instantaneous crystal growth breaks down. Instead, the U–Th data may be explained by continuous zircon growth over a period of ~ 90 ka. However, cathodoluminescence shows that crystals are typically composed of an euhedral core surrounded by a sector-zoned euhedral rim, and the U–Th data can also be modelled by mixing an older (~ 27 ka model age) population of zircon crystals with a young zircon rim that formed shortly prior to eruption of the Oruanui rhyolite. This indicates that detailed petrographic studies are critical for deciphering the histories of prolonged crystallisation in the magmatic environment. It is concluded that conventional U-series mineral isochrons may underestimate the age of the onset of crystallisation by more than an order of magnitude. In future, microanalytical techniques will lead to significant advances in the understanding of crystallisation processes and timescales. © 2000 Elsevier Science B.V. All rights reserved.

Keywords: geochronology; U-238/Th-230; isochrons; crystallization; zircon; Taupo volcanic zone; North Island

1. Introduction

Crystal residence times in crustal magma reservoirs are linked to rates and processes of magmatic evolution (see [1] for a recent review). Crystallisation is an inevitable consequence of magma

storage and processing in the crust. It may occur as a response to falling temperature, with the rate of crystallisation increasing with the rate of cooling. In addition, decompression may also play a major role, particularly in the formation of plagioclase crystals [2]. Further, magma degassing may result in extremely rapid crystallisation [3,4]. Conversely, crystallisation of accessory phases is often controlled by trace element solubility in the melt. For example, zircon crystallisation is dependent on the saturation state of Zr [5].

* Corresponding author. Tel.: +44-117-9545243;
Fax: +44-117-9253385; E-mail: georg.zellmer@bristol.ac.uk

Whatever the mechanism of crystallisation in any particular case, the result is a build up of volatiles in the liquid, which may in turn trigger explosive volcanic eruptions [6,7]. Thus, accurate dating of crystallisation events is critical to assess models of magma differentiation in crustal reservoirs, magma ascent through the crust, and links between crystallisation and volcanic eruptions.

U–Th dating of minerals was first employed more than three decades ago [8,9]. From the work of Taddeucci et al. [10] and Allègre [11] it became evident that the age yielded by an isochron through separated mineral phases from volcanic rocks may significantly predate the eruption age. Since then, U–Th dating of minerals in volcanic systems has yielded variable pre-eruptive crystal residence times ranging from ~ 0 ka, indicating crystallisation immediately prior to eruption, to > 100 ka for some rhyolitic systems, pointing to active magmatism over much longer periods of time [12–17]. In addition, Ra–Th mineral isochron dating has yielded model ages between 0 and 10 ka [18–20]. However, perfect U–Th isochrons are not always obtained without difficulties, particularly in cases where crystal residence times are variable, where xenocrysts are involved, or where more than one crystal population exist (cf. [19,21,22]).

Early studies using ^{230}Th – ^{238}U disequilibrium in zircon (e.g. [23,24]) highlighted the possibilities of using this mineral in dating silicic systems. Since U partitions to a greater extent than Th into the zircon lattice, large ^{238}U excesses in young zircons are observed, permitting good age resolution. In addition, U and Th concentrations in zircons are often 2–3 orders of magnitude higher than in the melt, so that less than ~ 1 mg of zircon separate is required for analysis. These advantages have been recognised before [15,16,22], but so far the low abundance of zircon in less evolved volcanic rocks has prevented the more widespread use of this mineral in U-series dating.

Using zircons from the 26.5 ka Oruanui eruption, Taupo Volcanic Zone, New Zealand (see [25] for details on this eruption), it can be demonstrated that the analysis of bulk separates alone will, in many cases, significantly underestimate the timing of the onset of crystallisation in the mag-

matic system under consideration. Additional techniques need to be employed to assess if conventional mineral isochrons yield meaningful ages. Petrographic studies are important, and here the distribution of crystal sizes in the analysed mineral separate is shown to also be critical in the interpretation of U-series mineral data. Finally, the implications of this study are not restricted to the dating of zircons, and the models presented may in principle be applicable to a variety of other mineral phases that show evidence for protracted growth histories.

2. Analytical techniques

A total of ~ 10 kg of rhyolitic pumice was crushed and sieved to obtain sub-63 μm , 63–125 μm and 125–250 μm size fractions. Preconcentration of heavy minerals was achieved using a laminar flow water fluidisation rig to produce density segregation between the mineral species and glass within the sieved powder samples. Remaining glass and light mineral phases were subsequently removed from the preconcentrated heavy material using heavy liquids. A preliminary zircon separate was obtained by magnetic separation. To remove adhering glass from the crystals, they were placed in dilute HF and HCl for 20 min. Hand picking was carried out as a final purification step and to remove damaged zircon crystals. A total of ~ 10 mg of zircon separates were thus obtained. Zircon size fractions were dissolved separately in Teflon bombs, and the U–Th composition of each size fraction was determined by TIMS following the procedure outlined in Turner et al. [26].

The distribution of crystal sizes and aspect ratios of the separated grains were determined by hand, using microscope photographs of each size fraction. Cathodoluminescence work was performed on selected grains at the University of Western Australia.

3. U–Th results

U–Th data of the whole-rock (WR) and three different zircon size fractions from the 26.3 ka

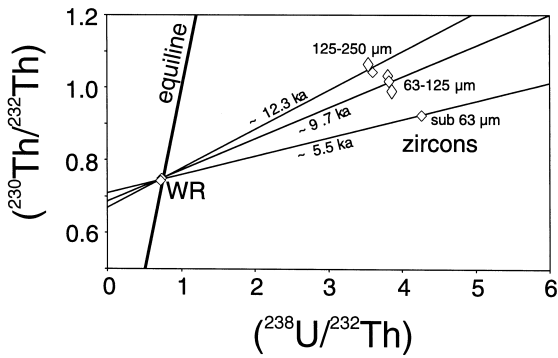


Fig. 1. U–Th equiline diagram with conventional WR–zircon two-point isochrons for the 26.5 ka Oruanui rhyolite at the time of eruption. Ages have been calculated using the program Isoplot [27]. The 63–125 μm size fraction data were reproduced twice, the 125–250 μm fraction and the WR once. Errors are smaller than symbol size. All reproduced zircon analyses are within 2σ error of each other.

Oruanui rhyolite, Taupo Volcanic Zone, New Zealand, are summarised in Table 1 and the U–Th compositions at the time of eruption are presented on an equiline diagram in Fig. 1. A complete dataset will be published elsewhere (Charlier et al., in preparation). Zircons are in $(^{230}\text{Th}/^{238}\text{U})$ disequilibrium, displaying large ^{238}U excesses. In addition, $(^{238}\text{U}/^{232}\text{Th})$ ratios decrease and $(^{230}\text{Th}/^{232}\text{Th})$ ratios increase with crystal size. Conventional WR–zircon isochrons were determined for each zircon size fraction using the program Isoplot [27], yielding pre-eruptive model ages of

5.5 ± 0.8 ka, 9.7 ± 1.7 ka and 12.3 ± 0.8 ka for the sub-63 μm, 63–125 μm and 125–250 μm fractions, respectively.

Conventional mineral isochrons are based on the assumptions that crystallisation occurs over a short time interval relative to the age of the crystals, and that the system was closed thereafter (e.g. [28]). This is clearly not the case, as all size fractions would then yield the same age. Thus, alternative explanations for the observed U–Th isotope data of the separated Oruanui zircons are required.

4. Alternative crystal growth models

4.1. Outline

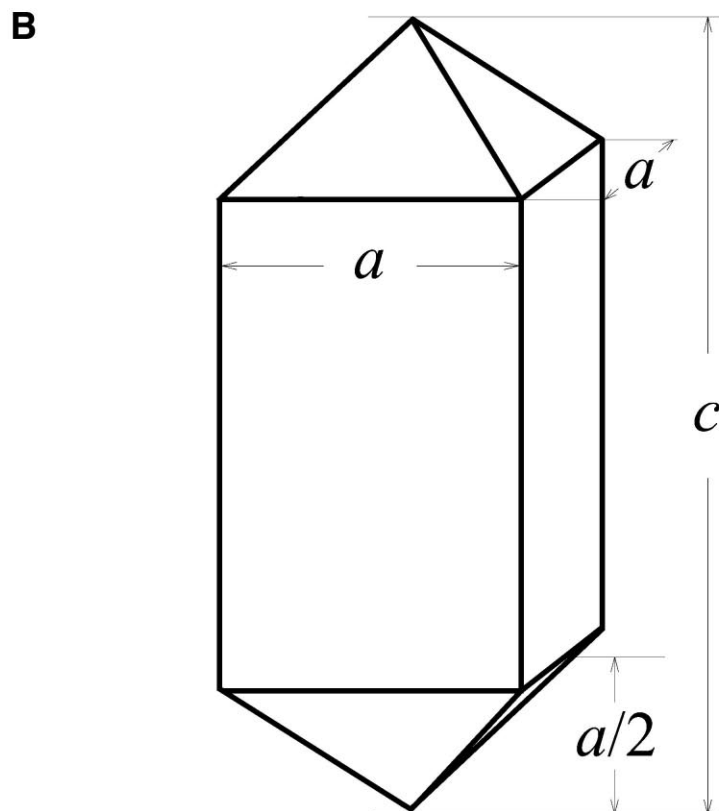
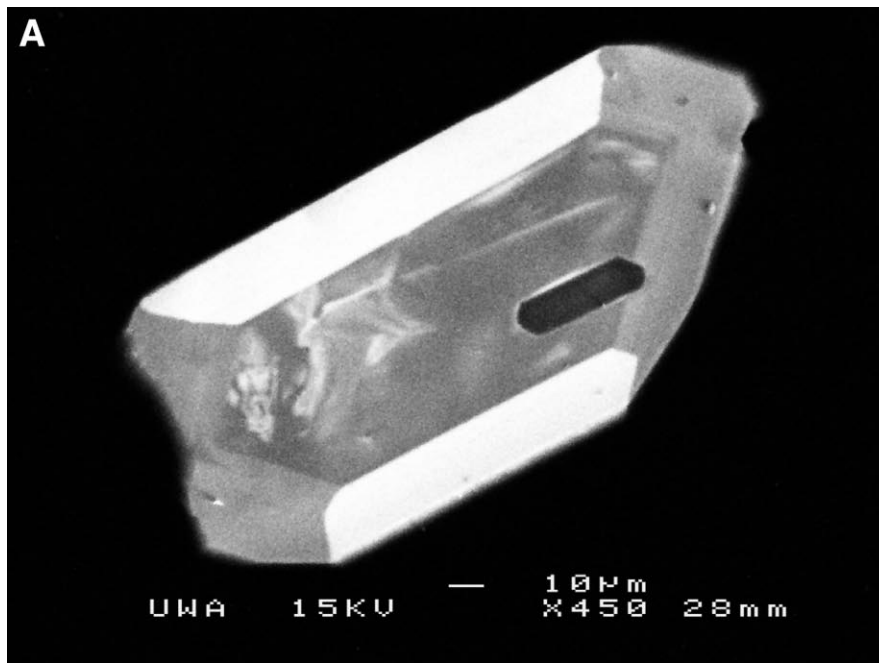
As rapid crystal growth and essentially instantaneous U–Th differentiation cannot reproduce the observed differences in $(^{230}\text{Th}/^{232}\text{Th})$ activity ratios of different size fractions, alternative crystal growth models need to be explored.

Continuous crystal growth (Section 4.2) was previously noted by Neymark and Paces [29] for Quaternary opals from Yucca Mountain, but in principle this concept can also be applied in long-lived magmatic environments with prolonged crystallisation histories. Initially, the volume (Section 4.2.1) and mean U–Th composition (Section 4.2.2) of each crystal are calculated. Then, crystals

Table 1
U–Th data and conventional mineral age for each analysed size fraction

| Sample | U (ppm) | Th (ppm) | $(^{238}\text{U}/^{232}\text{Th})$ | $\pm 2\sigma$ | $(^{230}\text{Th}/^{232}\text{Th})$ | $\pm 2\sigma$ | $(^{230}\text{Th}/^{232}\text{Th})_{\text{eruptive}}$ | $\pm 2\sigma$ | Isochron age (ka) |
|------------|---------|----------|------------------------------------|---------------|-------------------------------------|---------------|---|---------------|-------------------|
| WR | 2.37 | 10.0 | 0.719 | 0.007 | 0.738 | 0.009 | 0.743 | 0.012 | – |
| | 2.33 | 9.6 | 0.735 | 0.007 | 0.747 | 0.008 | 0.750 | 0.010 | – |
| sub-63 μm | 293 | 208 | 4.268 | 0.043 | 1.646 | 0.016 | 0.923 | 0.025 | 5.5 ± 0.8 |
| 63–125 μm | 272 | 213 | 3.863 | 0.039 | 1.611 | 0.016 | 0.990 | 0.024 | 9.7 ± 1.7 |
| | 291 | 231 | 3.826 | 0.038 | 1.625 | 0.016 | 1.018 | 0.024 | |
| | 276 | 220 | 3.812 | 0.038 | 1.634 | 0.016 | 1.033 | 0.024 | |
| 125–250 μm | 260 | 223 | 3.545 | 0.035 | 1.600 | 0.016 | 1.064 | 0.023 | 12.3 ± 0.8 |
| | 297 | 250 | 3.601 | 0.036 | 1.595 | 0.016 | 1.041 | 0.023 | |

An eruption age of 26500 ± 230 yr was used for the calculation of $(^{230}\text{Th}/^{232}\text{Th})_{\text{eruptive}}$, based on ^{14}C dating of Wilson et al. [39], recalibrated using the calibration curve of Bard [40].



are mixed according to the distribution of crystal sizes in each size fraction in order to model the U–Th composition of each analysed size fraction (Section 4.2.3). Thus it can be shown that young model ages may be an artefact of continuous crystallisation over a long time period.

Alternatively, episodic crystal growth (Section 4.3) may govern the observed range in U–Th composition of different size fractions. In this growth model, an older zircon crystal population is overgrown by a young zircon rim (Section 4.3.1), so that different size fractions are calculated to lie on a mixing line between the two end-members (Section 4.3.2).

It should be noted that the following models do not consider zircon dissolution. Dissolution could result from temporary Zr undersaturation, but there is no evidence for this in the Oruanui zircons. Rather, Zr shows compatible behaviour within the Oruanui rhyolite [30], and it can thus be assumed that zircon was a crystallising phase throughout the evolution of the magma.

Finally, diffusion of U and Th within the crystals and between the crystals and the melt was assumed to be negligible. Experimental data [31,32] suggest that diffusion coefficients of these cations in non-metamict zircons are so low that for growth rates exceeding 0.3 $\mu\text{m}/\text{kyr}$ zircons will behave as isotopically closed systems.

4.2. Modelling U-series responses to continuous crystal growth

4.2.1. Crystal geometry and volume

Zircon morphology is revealed by cathodoluminescence, which shows that crystals are typically composed of euhedral cores surrounded by sector-zoned euhedral rims (Fig. 2A). The reason for the occurrence of sector zoning in the rims is unclear, but sector zoning cannot be taken as evidence for

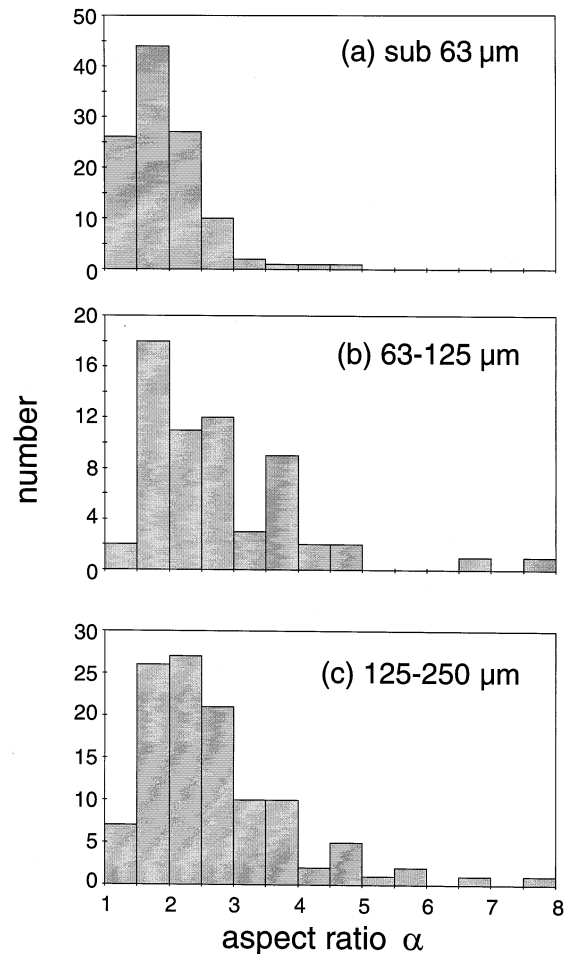


Fig. 3. Aspect ratio distribution of measured zircons for each size fraction. Their similarity suggests that the aspect ratio of a crystal is largely independent of its length.

rapid crystal growth [33]. Crystals are tetragonal, and their general geometry is shown in Fig. 2B. Taking a as width and c as total length of a crystal, crystal volumes are given by:

$$V = a^2 c - \frac{2}{3} a^3. \tag{1}$$

The aspect ratio $\alpha = c/a$ is variable, ranging from $\alpha \approx 1$ (approximately cubic crystals) to $\alpha \approx 8$ (needle-like crystals), with similar distributions of aspect ratios in each size fraction (Fig. 3a–c). For simplification, an aspect ratio of $\alpha \approx 2.62$ was chosen for the model. This is the

←
Fig. 2. (A) Morphology of an Oruanui zircon crystal, showing that crystals are euhedral without resorption surfaces. Crystal cores are typically surrounded by euhedral sector-zoned rims. A volumetrically negligible inclusion of apatite is visible in black. (B) Simplified zircon crystal geometry used in the model.

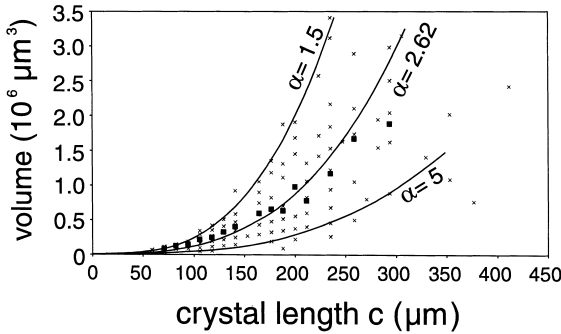


Fig. 4. Crystal volume versus length for all 287 measured crystals (×), contoured for aspect ratios. Mean volumes (■) have been calculated for cases where there were more than three crystals of a given length. Using the typical zircon geometry (Fig. 2), the average volume of a crystal of given length is readily approximated for an aspect ratio of 2.62.

aspect ratio that best approximates the mean crystal volumes at a given crystal length c (Fig. 4). It can be shown that the value of α chosen is of no importance in the model presented here, because it neither has an effect on the U–Th systematics nor on the modelled age of the pre-existing zircon population.

4.2.2. Evolution of the U–Th composition of a continuously growing crystal

In this simple crystal growth model, crystals are grown stepwise, with each growth zone having the same width. In each growth step, a new rim with $(^{230}\text{Th}/^{232}\text{Th})_{\text{rim}}$ equal to the $(^{230}\text{Th}/^{232}\text{Th})$ ratio of the decay-corrected WR value is formed around a crystal that has aged and ingrown ^{230}Th so that its $(^{230}\text{Th}/^{232}\text{Th})$ activity ratio is given by:

$$\left(\frac{^{230}\text{Th}}{^{232}\text{Th}}\right)_{\text{old}} = \left(\frac{^{230}\text{Th}}{^{232}\text{Th}}\right)_{\text{mean}} e^{-\lambda_{230}t} + \left(\frac{^{238}\text{U}}{^{232}\text{Th}}\right) (1 - e^{-\lambda_{230}t}) \quad (2)$$

where t is the time to grow the new zone and $(^{230}\text{Th}/^{232}\text{Th})_{\text{mean}}$ is the Th isotopic composition of the original crystal before it aged. The new mean $(^{230}\text{Th}/^{232}\text{Th})$ activity ratio of the grown crystal is then calculated by mixing the aged crystal with its new rim, so that:

$$\left(\frac{^{230}\text{Th}}{^{232}\text{Th}}\right)_{\text{mean}} = \left[\left(\frac{^{230}\text{Th}}{^{232}\text{Th}}\right)_{\text{old}} [\text{Th}]_{\text{old}} V_{\text{old}} + \left(\frac{^{230}\text{Th}}{^{232}\text{Th}}\right)_{\text{rim}} [\text{Th}]_{\text{rim}} V_{\text{rim}} \right] / V_{\text{total}} [\text{Th}]_{\text{mean}} \quad (3)$$

where $[\text{Th}]_{\text{mean}}$ is calculated from:

$$[\text{Th}]_{\text{mean}} = ([\text{Th}]_{\text{old}} V_{\text{old}} + [\text{Th}]_{\text{rim}} V_{\text{rim}}) / V_{\text{total}}. \quad (4)$$

(Note that decay correction of the WR ($^{230}\text{Th}/^{232}\text{Th}$) ratio to obtain $(^{230}\text{Th}/^{232}\text{Th})_{\text{rim}}$ is negligible if the WR is in or close to radioactive equilibrium as in the case of the Oruanui rhyolite.) Subsequently, $(^{230}\text{Th}/^{232}\text{Th})_{\text{new}}$ obtained in Eq. 3 is substituted into Eq. 2 and another new ring is grown in the next step. The evolution of the $(^{230}\text{Th}/^{232}\text{Th})$ activity ratio of the growing crystal with time depends on the rate of its crystallisation (and on the evolution of the WR if it is in U–Th disequilibrium).

So far only changes in Th isotopic composition have been taken into account. However, the Oruanui zircon data suggest that the U/Th ratio of the crystals also depends on crystal size, with larger crystals having lower ($^{238}\text{U}/^{232}\text{Th}$) activity ratios. This indicates that there is a general increase of U/Th ratios within the zircons from core to rim, assuming that smaller crystals nucleate later and therefore attain a composition similar to that of the rims of the larger crystals which have bulk lower ($^{238}\text{U}/^{232}\text{Th}$) activity ratios due to their low U/Th cores. With decreasing temperatures in a cooling magma, increasing U/Th ratios are consistent with changes in the relative partitioning of U and Th between zircon and melt in cases of equilibrium crystal growth (Blundy, personal communication, 2000), although more complicated variations in U–Th composition have been found before [34]. In the absence of any constraints, partitioning of U and Th between zircon

Table 2a
Continuous growth model

| Input parameters | |
|---|--------|
| dc/dt ($\mu\text{m}/\text{kyr}$) | 4.5 |
| $[\text{U}]_{\text{melt}}$ (ppm) | 2.370 |
| $[\text{Th}]_{\text{melt}}$ (ppm) | 9.630 |
| $(^{230}\text{Th}/^{232}\text{Th})_{\text{melt}}$ | 0.747 |
| $D_{\text{U,initial}}$ | 58 |
| dD_{U}/dt (kyr^{-1}) | 0.765 |
| $D_{\text{Th,initial}}$ | 47.8 |
| dD_{Th}/dt (kyr^{-1}) | −0.306 |

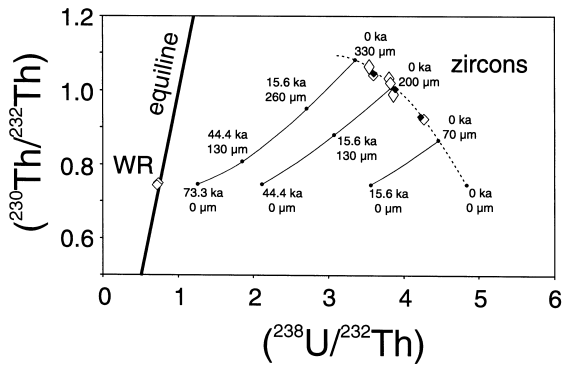


Fig. 5. Continuous crystal growth model on a U–Th equiline diagram with WR and zircon data as in Fig. 1. Thin lines represent the U–Th evolution of three representative crystals that have reached sizes of 330 μm , 200 μm and 70 μm at the time of eruption (0 ka), and have nucleated 73.3 ka, 44.4 ka and 15.6 ka prior to eruption, respectively. The last crystal that nucleated lies on point (0 μm , 0 ka). At the time of eruption all crystals lie on the dashed line, with both their $(^{238}\text{U}/^{232}\text{Th})$ and their $(^{230}\text{Th}/^{232}\text{Th})$ ratios depending on crystal size. The U–Th data (\diamond) of each size fraction can be modelled (\blacklozenge) by mixing crystals of different sizes according to the distribution of crystal sizes in each size fraction (Fig. 6), and by adjusting the model parameters (Table 2a).

and melt is taken to change linearly during crystal growth.

Selected crystal growth paths on the U–Th equiline diagram for crystals that at the time of eruption (0 ka) have reached sizes corresponding to lengths of 330 μm , 200 μm and 70 μm are shown on Fig. 5, using the parameters in Table 2a. The 330 μm crystal nucleated 73.3 ka prior to eruption, its core has a modelled $(^{238}\text{U}/^{232}\text{Th})$ ratio of ~ 1.27 . Crystals that nucleated later have progressively higher core $(^{238}\text{U}/^{232}\text{Th})$ ratios. The rim of all crystals has the same modelled $(^{238}\text{U}/^{232}\text{Th})$ ratio of 4.82 (0 ka, 0 μm). Crystals age as they grow, and thus the 330 μm crystal has a high $(^{230}\text{Th}/^{232}\text{Th})$ ratio as its core has ingrown significant ^{230}Th . Crystals that nucleated later have progressively lower $(^{230}\text{Th}/^{232}\text{Th})$ ratios.

4.2.3. Mixing crystals according to the distribution of crystal sizes in each size fraction

The dashed line on Fig. 5 indicates the U–Th trend displayed by crystals ranging in length from 412 μm (the largest Oruanui zircon measured)

down to 0 μm (just nucleating) at the time of eruption. To obtain the modelled U–Th compositions for each of the analysed size fractions, a volume-weighted mix of zircons of different sizes can now be calculated according to the distributions of their sizes in each size fraction (Fig. 6a–c), using the following relations:

$$[\text{U}]_{\text{mix}} = \frac{\sum_i [\text{U}]_{\text{mean},i} V_{\text{total},i} n_i}{\sum_i V_{\text{total},i} n_i} \quad (5)$$

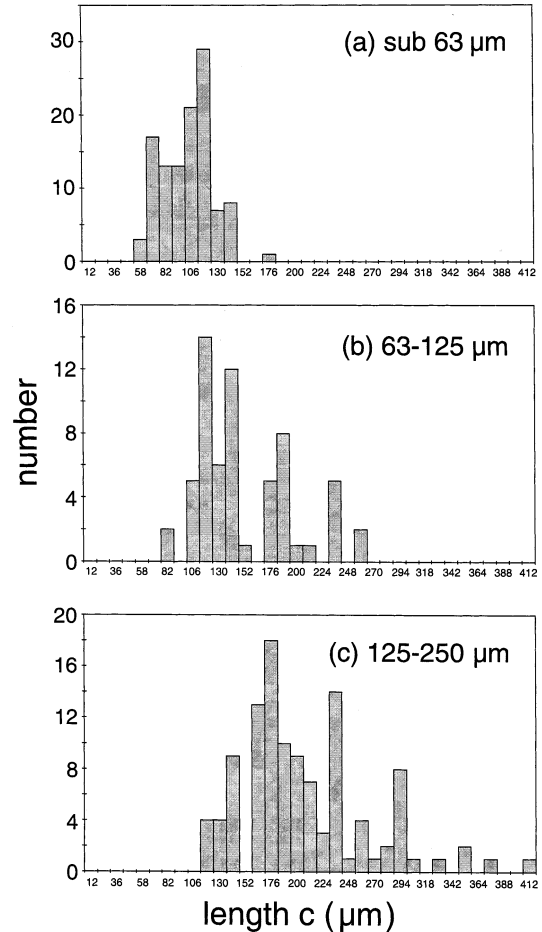


Fig. 6. The distribution of zircon crystal sizes for each size fraction. Measurements were made by hand from microscope photographs of the separated crystals. Note that there is significant overlap between different size fractions, and that the maximum crystal length in each size fraction is larger than the limiting mesh size. This can be attributed to the needle-like crystal geometry of some zircons (cf. Fig. 3).

$$[\text{Th}]_{\text{mix}} = \frac{\sum_i [\text{Th}]_{\text{mean},i} V_{\text{total},i} n_i}{\sum_i V_{\text{total},i} n_i} \quad (6)$$

$$(^{238}\text{U}/^{232}\text{Th})_{\text{mix}} = \{0.9677 \times [\text{U}]_{\text{mix}} \times \lambda_{238}\} / \{[\text{Th}]_{\text{mix}} \times \lambda_{232}\} \quad (7)$$

$$(^{230}\text{Th}/^{232}\text{Th})_{\text{mix}} = \frac{\sum_i (^{230}\text{Th}/^{232}\text{Th})_{\text{mean},i} [\text{Th}]_{\text{mean},i} V_{\text{total},i} n_i}{\sum_i [\text{Th}]_{\text{mean},i} V_{\text{total},i} n_i} \quad (8)$$

where i denotes the size fraction and n_i denotes the number of crystals in size fraction i . As crystals are elongated, crystals longer than the size of the mesh are found in each size fraction (Fig. 6a–c).

The modelled U–Th compositions of crystal mixes that represent the sub-63 μm , the 63–125 μm and the 125–250 μm size fractions are shown in Fig. 5. $D_{\text{U,initial}}$, dD_{U}/dt , $D_{\text{Th,initial}}$, dD_{Th}/dt and dc/dt are adjusted so that both isotopic compositions and [U] and [Th] concentrations of the data are reproduced by the model (Table 2b), with $D_{\text{U/Th}}$ increasing from 1.21 to 6.46. If the Oruanui zircons grew continuously rather than instantaneously, zircon crystallisation started ~ 90 ka prior to eruption (the calculated core age of the 412 μm crystal).

4.2.4. Uniqueness of the solution to the continuous growth model

As the U–Th composition of the melt is known and constant, growth rate and partitioning parameters are the only variables in this forward model. However, the choice of the partitioning parameters is governed by the known concentrations of U and Th within each size fraction, which the model has to reproduce. Changing D_{initial} will result in a proportional change in the modelled concentrations in all separates, while changing

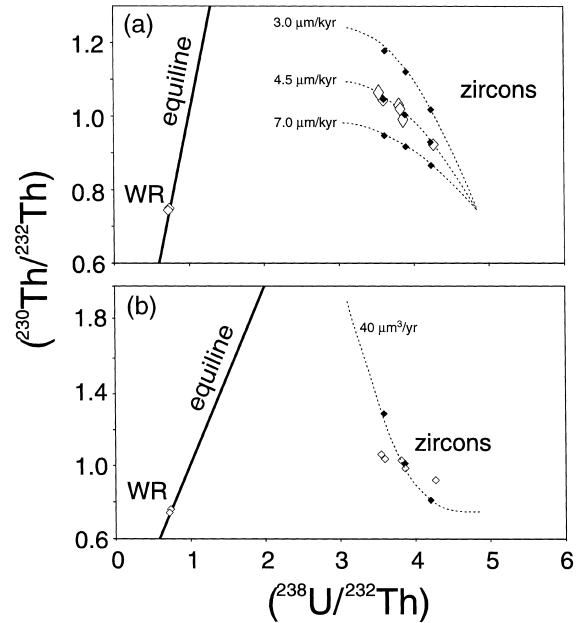


Fig. 7. Symbols as in Fig. 5. (a) Modelled U/Th compositions of crystals of different sizes at the time of eruption for growth rates of 3.0 $\mu\text{m}/\text{kyr}$, 4.5 $\mu\text{m}/\text{kyr}$ and 7.0 $\mu\text{m}/\text{kyr}$. Initial and final U and Th partition coefficients are the same in each model and are chosen to reproduce the observed U–Th composition of the separates. See text for details. (b) Constant growth rate in volumetric terms at 40 $\mu\text{m}^3/\text{yr}$. Errors on analyses are smaller than symbol size.

dD/dt will result in a change in the modelled range of concentrations. Thus, there is only one solution that describes the observed elemental composition of all three size fractions.

The choice of growth rate is governed by the Th isotopic composition of the separates. Fig. 7a shows the effect of varying growth rate. As growth rate increases, the residence times of crystals of a given size decrease and there is less time

Table 2b
Comparison of model results with data range (including 2 σ uncertainty)

| Results | U (ppm) | | Th (ppm) | | $(^{238}\text{U}/^{232}\text{Th})$ | | $(^{230}\text{Th}/^{232}\text{Th})$ | |
|-----------------------|---------|------------|----------|------------|------------------------------------|------------|-------------------------------------|------------|
| | Model | Data range | Model | Data range | Model | Data range | Model | Data range |
| sub-63 μm | 292 | 292–294 | 209 | 207–209 | 4.23 | 4.23–4.31 | 0.93 | 0.90–0.95 |
| 63–125 μm | 284 | 271–292 | 222 | 212–232 | 3.90 | 3.77–3.90 | 1.00 | 0.97–1.06 |
| 125–250 μm | 277 | 259–298 | 233 | 222–250 | 3.62 | 3.51–3.63 | 1.05 | 1.01–1.08 |

for ingrowth of ^{230}Th , resulting in lower modelled ($^{230}\text{Th}/^{232}\text{Th}$) ratios. Hence, in the continuous growth model only a small range of growth rates is capable to reproduce the data.

Finally, in the model presented here the growth rate is linear in terms of crystal dimension, implying that the rate of change of crystal volume accelerates during crystallisation. By gradually increasing the time required to form successive overgrowth rims of constant width, the model can be adjusted to a linear growth rate in volumetric terms. This was done in Fig. 7b, where partitioning parameters were chosen as above and growth rate was adjusted to model the ($^{230}\text{Th}/^{232}\text{Th}$) ratio of the intermediate size fraction. It is clear that constant growth rate in volumetric terms cannot reproduce the data as large old crystals acquire much too high ($^{230}\text{Th}/^{232}\text{Th}$) ratios relative to small young crystals. Although there may be other continuous growth models that successfully reproduce the data, choosing growth rate to be linear in terms of crystal dimension represents the simplest endmember case.

4.3. Overgrowing a pre-existing zircon population with a young rim

4.3.1. Mixing cores and rims on the equiline diagram

Cathodoluminescence and backscattered electron microscope images of the majority of Oruanui zircons reveal sector-zoned rims with widths of 10–15 μm . A couple of images suggest slightly wider rims of up to 35 μm , but as not all crystals may have been sectioned centrally, crystal rims were assumed to have a constant width of 10 μm . For given zircon core and rim compositions, the mean U–Th composition of a crystal can be calculated as a function of its size using the following relations:

$$[\text{U}]_{\text{mean}} = \{[\text{U}]_{\text{core}} \times V_{\text{core}} + [\text{U}]_{\text{rim}} \times V_{\text{rim}}\} / V_{\text{total}} \quad (9)$$

$$[\text{Th}]_{\text{mean}} = \{[\text{Th}]_{\text{core}} \times V_{\text{core}} + [\text{Th}]_{\text{rim}} \times V_{\text{rim}}\} / V_{\text{total}} \quad (10)$$

$$(^{238}\text{U}/^{232}\text{Th})_{\text{mean}} = \{0.9677 \times [\text{U}]_{\text{mean}} \times \lambda_{238}\} / \{[\text{Th}]_{\text{mean}} \times \lambda_{232}\} \quad (11)$$

$$\left(\frac{^{230}\text{Th}}{^{232}\text{Th}}\right)_{\text{mean}} = \frac{\{(^{230}\text{Th}/^{232}\text{Th})_{\text{core}} \times [\text{Th}]_{\text{core}} \times V_{\text{core}} + (^{230}\text{Th}/^{232}\text{Th})_{\text{rim}} \times [\text{Th}]_{\text{rim}} \times V_{\text{rim}}\}}{\{V_{\text{total}} \times [\text{Th}]_{\text{mean}}\}} \quad (12)$$

where $V_{\text{rim}} = V_{\text{total}} - V_{\text{core}}$. [U] and [Th] concentrations of core and rim are adjustable input parameters to the model and also determine the Th isotopic compositions of the endmembers that are constrained to lie on a mixing line through the data (cf. Fig. 8), described by:

$$(^{230}\text{Th}/^{232}\text{Th}) = 1.72 - 0.187(^{238}\text{U}/^{232}\text{Th}) \quad (13)$$

4.3.2. Mixing crystals according to the distribution of crystal sizes in each size fraction

The U–Th composition of a volume-weighted mix of zircons of different sizes can now be calculated according to the distributions of their sizes in each size fraction (Fig. 6a–c) as above (Section 4.2.3), using Eqs. 5–8. In principle, the crystal rim may have a ($^{230}\text{Th}/^{232}\text{Th}$) ratio between the WR value, representing rim growth just prior to eruption, and the composition of the sub-63 μm size fraction. Similarly, the core must have a composition between the 125–250 μm size fraction and the equiline, representing core growth greater than ~ 350 ka prior to eruption. However, Eq. 13 links ($^{230}\text{Th}/^{232}\text{Th}$) ratios and thus core and rim model ages to ($^{238}\text{U}/^{232}\text{Th}$) ratios, which in turn are determined by the U and Th concentrations in core and rim, respectively. As rim width is known and constant (10 μm), for any rim composition there exists a core composition that produces the observed bulk composition of a particular size fraction. However, with variable mean core volume but constant rim widths in each size fraction there cannot be more than one solution to reproduce the U–Th compositions of all size fractions.

The modelled U–Th compositions of crystal mixes that represent the sub-63 μm , the 63–125 μm and the 125–250 μm size fractions are shown in Fig. 8. For the input parameters in Table 3, the model results lie within the U–Th compositional range of the data. If the formation of both euhe-

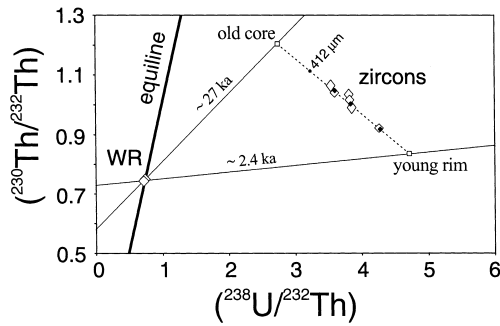


Fig. 8. Core-rim mixing model on a U-Th equiline diagram with WR and zircon data as in Fig. 1. All crystals lie on the dashed mixing line (cf. Eq. 13), with both their $(^{238}\text{U}/^{232}\text{Th})$ and their $(^{230}\text{Th}/^{232}\text{Th})$ ratio depending on crystal size. The U-Th data (\diamond) of each size fraction can be modelled (\blacklozenge) by mixing crystals of different sizes according to the distribution of crystal sizes in each size fraction (Fig. 6), and by adjusting the model parameters (Table 3). A WR-core isochron yields a model age of ~ 27 ka.

dral cores and sector-zoned euhedral rims occurred over a short timescale, conventional isochrons yield ages of 27 ka and 2.4 ka for cores and rims, respectively (Fig. 8). Even in this case the core age is significantly older than the ages obtained by conventional isochrons through the WR-zircon pairs (cf. Fig. 1). This result emphasises the importance of petrographic work when mineral isochron data are interpreted.

5. Discussion

From the forward models presented here, it can be seen how easy it is for mineral separates not to yield meaningful ages, and the simple assumption of rapid growth followed by ageing may be very misleading in the interpretation of crystallisation timescales in magmatic environments. Conventional mineral ages, mean ages of a set of separated crystals, and the total differentiation timescale depend on growth rates and the distribution of crystal sizes in the analysed separate and are compared in Fig. 9 using the size distributions in the Oruanui zircon separates. Fig. 9a shows that young conventional mineral ages may be taken as a good approximation for the mean age of a set of crystals. However, as the rims of crystals are volu-

metrically much more important than the cores, the onset of crystallisation will be significantly older than this mean age. It can be seen from Fig. 9b that conventional isochrons may underestimate the timescale of crystallisation by more than an order of magnitude.

This concept may be applied to the Oruanui zircon cores with an apparent age of ~ 27 ka (cf. Section 4.3.2). It is not possible to rule out continuous growth of the cores on the basis of the

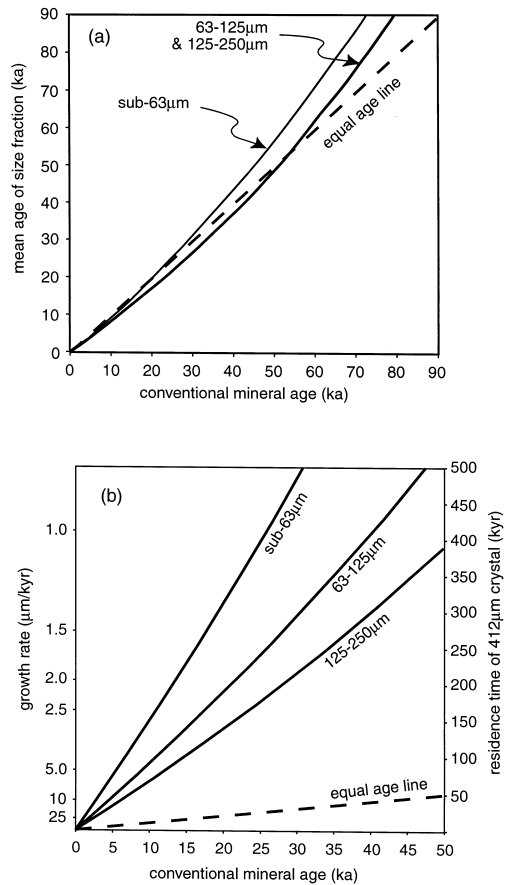


Fig. 9. (a) Comparison between the mean age of each size fraction and its conventional mineral age for the size distributions in Fig. 6. Young conventional isochrons (< 40 – 60 ka) approximate the mean age of the separate. (b) In the case of continuous growth, the conventional mineral age obtained depends on growth rate and the distribution of crystal sizes. The residence times for a $412 \mu\text{m}$ crystal such as the largest Oruanui zircon are given for reference. Conventional isochrons may underestimate the crystallisation timescale of the system by more than an order of magnitude.

Table 3

Mixing model input parameters (in bold), calculated U–Th isotope composition on the basis of a mixing line with slope -0.187 and intercept 1.72 , and comparison of model results with data range (including 2σ uncertainty)

| | U (ppm) | Th (ppm) | | | $(^{238}\text{U}/^{232}\text{Th})$ | | $(^{230}\text{Th}/^{232}\text{Th})$ | |
|-----------------------|------------|-------------|-------|------------|------------------------------------|------------|-------------------------------------|------------|
| Input parameters | | | | | | | | |
| core | 257 | 280 | | | 2.79 | | 1.20 | |
| rim | 300 | 192 | | | 4.74 | | 0.835 | |
| Results | Model | Data range | Model | Data range | Model | Data range | Model | Data range |
| sub-63 μm | 293 | 292–294 | 207 | 207–209 | 4.30 | 4.23–4.31 | 0.92 | 0.90–0.95 |
| 63–125 μm | 284 | 271–292 | 224 | 212–232 | 3.85 | 3.77–3.90 | 1.00 | 0.97–1.06 |
| 125–250 μm | 279 | 259–298 | 235 | 222–250 | 3.60 | 3.51–3.63 | 1.05 | 1.01–1.08 |

available data. The zircon core composition obtained in Section 4.3 may be modelled by continuous growth, with D_{U} and D_{Th} kept constant such that the U and Th concentrations of the modelled core are reproduced (cf. Table 3). As all rhyolite WR samples from Taupo Volcanic Centres are close to U–Th radioactive equilibrium with $(^{230}\text{Th}/^{232}\text{Th})$ activity ratios only ranging from ~ 0.7 to ~ 0.8 (Charlier, unpublished data), the same U–Th melt composition as in Table 2a may be used. Finally, an appropriate distribution of core sizes needs to be chosen. The distribution of crystal sizes was only determined separately for each size fraction, and the 125–250 μm size fraction is used here, although this will lead to an underestimate of the age of onset of crystallisation, because a number of small, young crystals with low $(^{230}\text{Th}/^{232}\text{Th})$ ratios are unaccounted for. The distribution of core sizes is determined by subtracting the total length of the sector-zoned rims ($2\alpha \times 10 \mu\text{m}$) from each crystal. The overall ingrowth of ^{230}Th in a continuously growing crystal is solely governed by its growth rate, which has to be adjusted to obtain a core $(^{230}\text{Th}/^{232}\text{Th})$ ratio of 1.2 (cf. Fig. 8). A growth rate of $2.1 \mu\text{m/kyr}$ is obtained, implying an age greater than 170 ka for the onset of crystallisation of the longest, 360 μm long core ($412 \mu\text{m} - 2\alpha \times 10 \mu\text{m}$). Note that this age is more than an order of magnitude older than 12.3 ka, the age yielded by a conventional isochron through the 125–250 μm size fraction.

It follows that bulk dissolution techniques in geochronology may result in ambiguities that can-

not be resolved without a good knowledge of the chemical heterogeneity within a crystal population and the distribution of crystal sizes. Conventional model ages from bulk mineral separates generally underestimate the timing of the onset of crystallisation significantly. In consequence, future advances in U-series geochronology are likely to be achieved by employing microanalytical techniques in conjunction with the methods presented here. U–Pb data from ion microprobe spot analyses of cores and rims of magmatic zircons have previously been used to assess the pre-eruptive crystallisation histories of older high-Si rhyolites such as the ~ 340 ka Whakamaru Ignimbrite, New Zealand [35], and the ~ 760 ka Bishop Tuff [36]. However, dating of these older deposits is limited by analytical uncertainties that preclude a very precise determination of pre-eruptive crystallisation timescales. With further developments in microanalytical techniques it may in the future be possible to determine U/Th isotopic variations across single crystals and to extend the microprobe dating techniques to progressively younger systems.

Finally, it should be noted that the arguments outlined in this contribution are also applicable to other mineral phases that are generally used in U-series isochron studies. Most importantly, Ra–Th plagioclase–WR model ages [18] probably underestimate the age of onset of crystallisation given the complexities of plagioclase morphology, where multiple resorption events can frequently be observed using Nomarski interferometry [37,38]. In this case a young overgrowth rim on

plagioclase crystals that are tens of thousands of years in age may produce ^{226}Ra excesses that result in model ages of a few thousand years.

6. Conclusions

Minerals often have complex growth histories revealed by their crystal morphology. Crystal growth may occur in episodes or continuously. The detailed growth history of a crystal population becomes very important when short-lived isotope systems (e.g. the U-series system) are employed in geochronology, because then the timescale of crystallisation and the half-life of the radioactive daughter are of similar order. Zircons from the Oruanui rhyolite, Taupo Volcanic Zone, serve as an example to show that conventional WR–mineral isochrons yield pre-eruptive model ages (ranging from ~ 5.5 ka to ~ 12.3 ka) that significantly underestimate the age of onset of crystallisation which may have been at least 27 ka prior to eruption. In the case of continuous crystal growth, the timing of initial crystal nucleation may exceed the pre-eruptive model age derived from conventional isochrons by more than an order of magnitude.

In summary, a detailed knowledge of the morphology of analysed crystals, the chemical heterogeneity within crystals, and the distribution of crystal sizes in the separate is required to obtain more robust estimates of pre-eruptive crystallisation timescales. Mineral microanalyses may in future significantly improve our understanding of the detailed crystallisation histories of magmatic systems.

Acknowledgements

We would like to acknowledge the particularly constructive comments of Steve Blake and the thought-provoking discussions with Simon Turner. Chris Hawkesworth and Simon Turner are thanked for careful informal reviews, and John Blundy, Gavin Foster, Rob Hughes, Peter van Calsteren and Colin Wilson for their helpful thoughts. Furthermore, we wish to thank Stuart

Brown, Peter van Calsteren, Mabs Gilmour, Jo Rhodes and Colin Wilson for their support during the analytical work. This manuscript benefited from critical reviews by Bernard Bourdon, David Pyle and James Gill, and we thank Alex Halliday for speedy editorial handling. B.C. was funded by an Open University studentship and G.Z. by a Leverhulme Research Grant. [AHJ]

References

- [1] C.J. Hawkesworth, S. Blake, P. Evans, R. Hughes, R. Macdonald, L.E. Thomas, S.P. Turner, G.F. Zellmer, Time scales of crystal fractionation in magma chambers – integrating physical, isotopic and geochemical perspectives, *J. Petrol.* 41 (7) (2000) 991–1006.
- [2] K. Cashman, J. Blundy, Degassing and crystallization of ascending andesite and dacite, *Phil. Trans. R. Soc. A* 358 (2000) 1443–1464.
- [3] C.H. Geschwind, M.J. Rutherford, Crystallisation of microlites during magma ascent – the fluid-mechanics of 1980–1986 eruptions at Mount-St.-Helens, *Bull. Volcanol.* 57 (1995) 356–370.
- [4] J.G. Brophy, C.S. Whittington, J.-R. Park, Sector-zoned augite megacrysts in Aleutian high alumina basalts: Implications for the conditions of basalt crystallization and the generation of calc-alkaline series magmas, *Contrib. Mineral. Petrol.* 135 (1999) 277–290.
- [5] E.B. Watson, Dissolution, growth and survival of zircons during crustal fusion: kinetic principles, geological models and implications for isotopic inheritance, *Trans. R. Soc. Edinb. Earth Sci.* 87 (1996) 43–56.
- [6] S. Tait, C. Jaupart, S. Vergnolle, Pressure, gas content and eruption periodicity of a shallow, crystallizing magma chamber, *Earth Planet. Sci. Lett.* 92 (1989) 107–123.
- [7] R.S.J. Sparks, Causes and consequences of pressurisation in lava dome eruptions, *Earth Planet. Sci. Lett.* 150 (1997) 177–189.
- [8] E. Cerrai, R. Dugnani-Lonati, F. Gassarrini, E. Tongiorgi, Il metodo ionio/uranio per la determinazione dell'età di minerali vulcanici recenti, *Rend. Soc. Mineral. Ital.* 21 (1965) 47–62.
- [9] K. Kigoshi, Ionium dating of igneous rocks, *Science* 156 (1967) 932–934.
- [10] A. Taddeucci, W.S. Broecker, D.L. Thurber, ^{230}Th dating of volcanic rocks, *Earth Planet. Sci. Lett.* 3 (1967) 338–342.
- [11] C.J. Allègre, ^{230}Th dating of volcanic rocks: a comment, *Earth Planet. Sci. Lett.* 5 (1968) 209–210.
- [12] C.J. Allègre, M. Condomines, Fine chronology of volcanic processes using ^{238}U – ^{230}Th systematics, *Earth Planet. Sci. Lett.* 28 (1976) 395–406.
- [13] M. Condomines, C.J. Allègre, Age and magmatic evolu-

- tion of Stromboli Volcano from ^{230}Th – ^{238}U data, *Nature* 288 (1980) 354.
- [14] M. Condomines, J.-C. Tanguy, G. Kiefer, C.J. Allègre, Magmatic evolution of a volcano studied by ^{230}Th – ^{238}U disequilibrium and trace element systematics: the Etna case, *Geochim. Cosmochim. Acta* 46 (1982) 1397–1416.
- [15] M. Condomines, Dating recent volcanic rocks through ^{230}Th – ^{238}U disequilibrium in accessory minerals: Example of the Puy de Dome (French Massif Central), *Geology* 25 (4) (1997) 375–378.
- [16] M.R. Reid, C.D. Coath, T.M. Harrison, K.D. McKeegan, Prolonged residence times for the youngest rhyolites associated with Long Valley Caldera: ^{230}Th – ^{238}U ion microprobe dating of young zircons, *Earth Planet. Sci. Lett.* 150 (1997) 27–39.
- [17] E. Heath, S. Turner, R. Macdonald, C.J. Hawkesworth, P. van Calsteren, Long magma residence times at an island arc volcano (Soufriere, St. Vincent) in the Lesser Antilles: evidence from ^{238}U – ^{230}Th isochron dating, *Earth Planet. Sci. Lett.* 160 (1998) 49–63.
- [18] M.K. Reagan, A.M. Volpe, K.V. Cashman, ^{238}U - and ^{232}Th -series chronology of phonolite fractionation at Mount Erebus, Antarctica, *Geochim. Cosmochim. Acta* 56 (1992) 1401–1407.
- [19] A.M. Volpe, P.E. Hammond, ^{238}U – ^{230}Th – ^{226}Ra disequilibria in young Mount St. Helens rocks: time constraint for magma formation and crystallisation, *Earth Planet. Sci. Lett.* 107 (1991) 475–486.
- [20] A.M. Volpe, ^{238}U – ^{230}Th – ^{226}Ra disequilibrium in young Mt. Shasta andesites and dacites, *J. Volcanol. Geotherm. Res.* 53 (1992) 227–238.
- [21] B. Bourdon, A. Zindler, G. Wörner, Evolution of the Laacher See magma chamber: Evidence from SIMS and TIMS measurements of U–Th disequilibria in minerals and glasses, *Earth Planet. Sci. Lett.* 126 (1994) 75–90.
- [22] D.M. Pyle, M. Ivanovich, R.S.J. Sparks, Magma cumulate mixing identified by U–Th disequilibrium dating, *Nature* 331 (1988) 157–159.
- [23] T. Fukuoka, Ionium dating of acidic volcanic rocks, *Geochem. J.* 8 (1974) 109–116.
- [24] T. Fukuoka, K. Kigoshi, Discordant Io-ages and the uranium and thorium distribution between zircon and host rocks, *Geochem. J.* 8 (1974) 117–122.
- [25] C.J.N. Wilson, The 26.5 ka Oruanui eruption, New Zealand: an introduction and overview, *J. Volcanol. Geotherm. Res.* (2000), submitted.
- [26] S. Turner, C. Hawkesworth, P. van Calsteren, E. Heath, R. Macdonald, S. Black, U-series isotopes and destructive plate margin magma genesis in the Lesser Antilles, *Earth Planet. Sci. Lett.* 142 (1–2) (1996) 191–207.
- [27] K.R. Ludwig, Isoplot/Ex ver. 2.22, A Geochronological Toolkit for Microsoft Excel, Berkeley Geochronology Centre, Berkeley, CA, 2000.
- [28] G. Faure, Principles of Isotope Geology, Wiley, 1977, 589 pp.
- [29] L.A. Neymark, J.B. Paces, Consequences of slow growth for ^{230}Th /U dating of Quaternary opals, Yucca Mountain, NV, USA, *Chem. Geol.* 164 (1–2) (2000) 143–160.
- [30] A.N. Sutton, S. Blake, C.J.N. Wilson, An outline geochemistry of rhyolite eruptives from Taupo volcanic centre, New Zealand, *J. Volcanol. Geotherm. Res.* 68 (1995) 153–175.
- [31] D.J. Cherniak, J.M. Hanchar, E.B. Watson, Diffusion of tetravalent cations in zircon, *Contrib. Mineral. Petrol.* 127 (1997) 383–390.
- [32] J.K.W. Lee, I.S. Williams, D.J. Ellis, Pb, U and Th diffusion in natural zircon, *Nature* 390 (1997) 159–162.
- [33] E.B. Watson, Y. Liang, A simple model for sector zoning in slowly grown crystals: Implications for growth rate and lattice diffusion, with emphasis on accessory minerals in crustal rocks, *Am. Mineral.* 80 (1995) 1179–1187.
- [34] A. Benisek, F. Finger, Factors controlling the development of prism faces in granite zircons: a microprobe study, *Contrib. Mineral. Petrol.* 114 (1993) 441–451.
- [35] S.J.A. Brown, I.R. Fletcher, SHRIMP U–Pb dating of the preeruption growth history of zircons from the 340 ka Whakamaru Ignimbrite, New Zealand: Evidence for > 250 k.y. magma residence times, *Geology* 27 (11) (1999) 1035–1038.
- [36] M.R. Reid, C.D. Coath, In situ U–Pb ages of zircons from the Bishop Tuff: No evidence for long crystal residence times, *Geology* 28 (5) (2000) 443–446.
- [37] T.H. Pearce, A.M. Kolisnik, Observations of plagioclase zoning using interference imaging, *Earth Sci. Rev.* 29 (1–4) (1990) 9–26.
- [38] B.S. Singer, M.A. Dungan, G.D. Layne, Textures and Sr, Ba, Mg, Fe, K, and Ti compositional profiles in volcanic plagioclase: Clues to the dynamics of calc-alkaline magma chambers, *Am. Mineral.* 80 (1995) 776–798.
- [39] C.J.N. Wilson, V.R. Switsur, A.P. Ward, A new C-14 age for the Oruanui (Wairakei) eruption, New Zealand, *Geol. Mag.* 125 (1988) 297–300.
- [40] E. Bard, Geochemical and geophysical implications of the radiocarbon calibration, *Geochim. Cosmochim. Acta* 62 (1998) 2025–2038.